nanomaterials

MDPI

Article

Electrochemical Deposition of Gold Nanoparticles on Reduced Graphene Oxide by Fast Scan Cyclic Voltammetry for the Sensitive Determination of As(III)

Guo Zhao [1,2] and Gang Liu [1,2,*]

[1] Key Laboratory of Modern Precision Agriculture System Integration Research, Ministry of Education of China, China Agricultural University, Beijing 100083, China; guozhao1989@gmail.com

[2] Key Laboratory of Agricultural Information Acquisition Technology, Ministry of Agriculture of China, China Agricultural University, Beijing 100083, China

* Correspondence: pac@cau.edu.cn; Tel.: +86-010-6273-6741

Received: 8 November 2018; Accepted: 24 December 2018; Published: 29 December 2018

Abstract: In this study, a stable, sensitive electrochemical sensor was fabricated by the electrochemical codeposition of reduced graphene oxide (rGO) and gold nanoparticles on a glassy carbon electrode (rGO-Au_{nano}/GCE) using cyclic voltammetry (CV), which enabled a simple and controllable electrode modification strategy for the determination of trace As(III) by square wave anodic stripping voltammetry (SWASV). SWASV, CV, electrochemical impedance spectroscopy (EIS), X-ray diffraction (XRD) and scanning electron microscopy (SEM) were used to characterize the electrochemical properties and morphology of the proposed sensing platform. The number of sweep segments, the deposition potential and the deposition time were optimized to obtain ideal sensitivity. The presence of rGO from the electroreduction of graphene oxide on the sensing interface effectively enlarged the specific surface area and consequently improved the preconcentration capacity for As(III). The rGO-Au_{nano}/GCE sensor exhibited outstanding detection performance for As(III) due to the combined effect of Au_{nano} and rGO formed during the electroreduction process. Under the optimized conditions, a linear range from 13.375 $\times$ 10^{-9} to 668.75 $\times$ 10^{-9} mol/L (1.0 to 50.0 μg/L) was obtained with a detection limit of 1.07 $\times$ 10^{-9} mol/L (0.08 μg/L) (S/N = 3). The reproducibility and reliability of the rGO-Au_{nano}/GCE sensor were also verified by performing 8 repetitive measurements. Finally, the rGO-Au_{nano}/GCE sensor was used for the analysis of real samples with satisfactory results.

Keywords: reduced graphene oxide; gold nanoparticle; square wave anodic stripping voltammetry; arsenic detection; soil

1. Introduction

While As(III) is one of the most toxic forms of arsenic, even at low concentrations, it is widespread in natural environments [1,2]. As(III) contamination in agricultural soil is a serious problem because the presence of As in the food chain can cause many health problems [3,4], such as bladder cancer, lung cancer, keratosis and skin lesions. Therefore, the development of a simple, fast and sensitive method for the determination of As(III) in soil is urgently needed. Generally, there are two types of analytical strategies for the detection of As(III): spectroscopic and electrochemical methods. Spectroscopic methods, such as inductively coupled plasma mass spectrometry [5], atomic absorption spectroscopy [6] and hydride generation atomic fluorescence spectrometry [7], have very high detection accuracy. However, these methods require expensive instruments, long analysis times, and laboratory conditions. They are not suitable for on-site analyses and routine monitoring, especially for large

numbers of samples. In contrast, one electrochemical method, anodic stripping voltammetry (ASV), has been widely used for trace analyses of metal ions in different environments and industry samples due to its outstanding analytical performance, low cost, convenient operation and high sensitivity. ASV mainly consists of two steps [8]: preconcentration and stripping. The target metals are electrodeposited on the working electrode surface under a reduction potential in the preconcentration step. Then, the metals preconcentrated on the electrode surface are oxidized into their cationic forms under a scanning potential, and the concentration of the target heavy metal is proportional to the stripping response current. Therefore, the working electrode substrate plays a key role in improving the detection sensitivity of this technique.

Dropping mercury electrodes have frequently been used with stripping voltammetry for the analysis of heavy metals due to their high sensitivity and reproducibility. However, because of their operational limitations and potential toxicity, electrochemical sensors that use dropping mercury electrodes as the working electrode have been gradually replaced by sensors with solid electrodes. ASV with gold nanomaterial-modified electrodes has been widely applied for the determination of As(III) [9,10], and gold has already been verified to improve the sensitivity of a bare electrode by the electrogeneration of H_2 [11]. Gold nanoparticles can be made by chemical synthesis [12,13], ultraviolet (UV) light [14], electron-beam irradiation [15] or electrochemical methods [16,17].

Some reports have indicated the cathodic formation of a single As(0) monolayer on an Au surface, possibly due to the nonconducting nature of As(0) deposits. Because As(0) deposits are nonconductive, increasing the specific surface area is very important to improve the ASV analysis sensitivity for As(III). Li et al. reported a facile and green approach for fabricating Au-reduced graphene oxide (Au-rGO) nanocomposites by UV irradiation to detect As(III) [14]. The mixture of GO and $HAuCl_4$ was irradiated with a high-intensity UV spot lamp, while nitrogen was bubbled through the solution to activate the reduction reaction. After 20 min of irradiation, the product was separated by centrifugation and washed with water. Next, the sample was redispersed in water and used to modify an electrode surface for the detection of As(III). Electrodeposition is a cost-effective approach to rapidly and directly grow Au nanoparticles in an aqueous solution. The interplay between the crystal growth rate and the mass transport rate in the electrocrystallization can be readily manipulated via the control of deposition potential without changing the reactant concentration [18–20]. Recently, an electrochemical reduction strategy was developed and further applied to the modification of graphene using graphene oxide (GO). The results demonstrated that GO can be reduced on the surface of an electrode to form one or several graphene layers with a controllable potential, such as those used in cyclic voltammetry (CV) and potentiostatic methods [21]. Hence, based on the discussion above, the preparation and modification of reduced GO (rGO) and Au_{nano} by a one-step coelectrodeposition process to form a rGO-Au_{nano} sensing interface is possible because under cathodic conditions, both metal ions and GO have the ability to obtain electrons and activate reduction reactions, as reported in reference [22]. Additionally, the thickness of the Au-rGO nanocomposite film formed on the electrode surface can be controlled by the deposition time. After the optimization of the deposition time, the total time needed for the preparation of nanocomposite and modification of the electrode is 120 s, which is far less than the time for the ultraviolet irradiation method. Clearly, compared to the ultraviolet irradiation method electrochemical deposition is a fast, easy, convenient and effective method that does not require special instruments for the preparation of Au-rGO nanocomposite films [23].

In this study, we attempted to develop a rGO-Au_{nano} nanocomposite with a high specific surface area and excellent catalytic performance using solution-dispersed GO and $HAuCl_4$ with CV, which is a controllable technique that produces sensitive, homogeneous and stable sensing interfaces. The proposed rGO-Au_{nano}-modified glassy carbon electrode (GCE) exhibited high sensitivity and stability due to the combined effect of the rGO and Au_{nano} formed via electrochemical reduction, outstanding catalytic ability for As(III) and good electrical conductivity. The electrochemical analysis parameters, i.e., the number of sweep segments, deposition potential and deposition time, were optimized. Interference from nontarget heavy metals and the repeatability of the developed electrochemical platform were

also investigated. Finally, the fabricated rGO-Au_{nano}/GCE was applied for the analysis of trace As(III) in real soil samples by SWASV with satisfactory results.

2. Materials and Methods

2.1. Materials

$HAuCl_4$ was purchased from Sinopharm Chemical Reagent Co., Ltd. (c). Arsenic trioxide (As_2O_3) was purchased from Aldrich (Sigma-Aldrich, Saint Louis, MO, USA) and then dissolved in 1.0 M aqueous NaOH to create a 1000 mg/L solution. GO was obtained from Nanjing JCNANO Materials Tech Co., Ltd. (Nanjing, China). A nitric acid solution (1.0 M) was used as the supporting electrolyte during the stripping voltammetry analysis of As(III). Millipore-Q (18.2 MΩ) water was used for all experiments.

2.2. Instrument

Scanning electron microscopy (SEM) was performed on a NovaNanoSEM 450 scanning electron microscope. X-ray diffraction (XRD) patterns of Au_{nano} were obtained with a PANalytical Empyrean Series 2 X-ray diffractometer in the 2θ range from 30° to 90°. The electrochemical measurements and analyses, such as electrochemical impedance spectroscopy (EIS), CV and SWASV, were carried out using a CHI660D electrochemical workstation (Shanghai CH Instruments, Shanghai, China). A Pt wire electrode, Ag/AgCl electrode and GCE (ø3 mm) were used as the counter, reference and working electrodes, respectively, to construct a three-electrode system. A 25 mL beaker was used as the electrolytic cell for all electrochemical measurements. A magnetic stirrer was used to stir the test solution during the deposition step.

2.3. Synthesis and Modification of the rGO-Au_{nano} Nanocomposite

Prior to modification, the GCE surface was polished using 0.05 mm alumina powder, and the electrode was then sonicated in 1:1 HNO_3, absolute ethanol and water in sequence to remove alumina residue. GO was dispersed in a PBS solution (0.1 M, pH 9.0) by ultrasonication to form a GO dispersion with a concentration of 0.1 mg/mL. $HAuCl_4$ was added to the GO suspension to form 0.1 mM Au^{3+}, and then nitrogen purging was performed for 1 h to deoxygenate the solution and exfoliate the stacked GO. CV electrodeposition was carried out at a scan rate of 50 mV/s in the potential range from −1.4 to 0.6 V for 10 sweep segments (i.e., 5 cycles). After electrodeposition, the rGO-Au_{nano}/GCE was gently washed with ultrapure water. The same procedures described above were used to prepare the other electrodes.

2.4. Electrochemical Detection of As(III)

The SWASV measurements for As(III) detection were carried out based on a three-electrode system that used the rGO-Au_{nano}/GCE as the working electrode under the optimized conditions. A deposition potential of −0.3 V vs. Ag/AgCl was applied to the as-prepared rGO-Au_{nano}/GCE for 250 s in a nitric acid solution (0.1 M) with stirring during the deposition step. After equilibration for 10 s, the stripping voltammogram was recorded from −0.2 to 0.4 V vs. Ag/AgCl with a step potential of 5 mV, a pulse amplitude of 25 mV and a frequency of 25 Hz. An activation process was initiated in the nitric acid solution (0.1 M) to clean the electrode surface and remove previous residual As(0) using a constant positive potential of 0.6 V for 120 s. For comparison, the same process and conditions were used for the other modified electrodes.

2.5. Soil Sample Preparation

The soil samples were obtained from farmland in China. The detailed process is as follows: first, 40 mL of 0.1 M nitric acid was mixed with a 10 g soil sample using strong shaking. Then, a portable ultrasonic extractor was used to sonicate the above mixture for 10 min. After that, the obtained mixed

solution was centrifuged (2000 rpm) using a portable centrifuge, and then, 20 mL of supernatant was loaded into a 30 mL electrolyte cell for the SWASV measurements. Krasnodêbska-Ostrêga and Kowalska [24] verified that there is no significant difference between the ultrasonic-assisted extraction method and the method proposed by the European Communities Bureau of Reference.

3. Results and Discussion

3.1. Electrochemical Deposition of the rGO-Au$_{nano}$ Composite

The CV electroanalysis curves of GO on a GCE can be seen in Figure 1A, and one oxidation peak (a) and two reduction peaks (b and c) can be observed. The peak currents increased with successive potential scans, demonstrating that GO was successfully electrochemically reduced on the electrode surface. The current peak (c) was due to the reduction of the oxygen-containing groups on GO [25–27]. The peak currents that appeared at positions "a" and "b" were due to the redox reaction of some redox pairs on the graphene plane, and peak "c" was attributed to the irreversible electrochemical reduction of GO [28].

The CV curve for the electroanalysis of 0.1 mM $HAuCl_4$ is shown in Figure 1B. A significant reduction peak is present at approximately 0.18 V, indicating that the gold salt was reduced from Au^{3+} to Au^0. The electrochemical reduction of Au_{nano} on the electrode surface would be an outstanding active site for the reduction of Au^{3+} to Au^0. The CV electroanalysis results for the mixture of GO and $HAuCl_4$ are shown in Figure 1C, and these results were completely different from those observed for the GO electroanalysis. One significant difference is that the currents from scanning at a positive potential to scanning at a negative potential in the range of −1.2 V to −1.4 V for the mixture of GO and $HAuCl_4$ were dramatically larger than those obtained the GO electroanalysis, indicating the continuous electrodeposition of Au_{nano}, which is more conductive than rGO, onto the electrode surface.

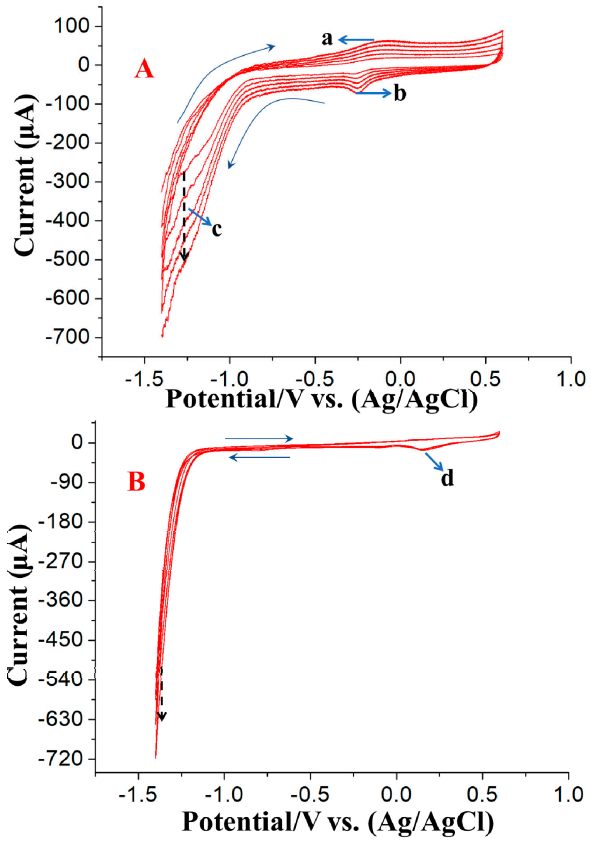

Figure 1. *Cont.*

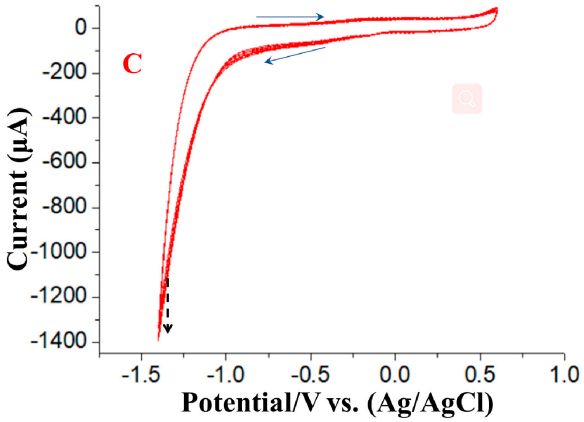

Figure 1. CV curves for the electroanalysis of (**A**) 0.1 mg/mL GO, (**B**) 0.1 mM $HAuCl_4$ and (**C**) 0.1 mg/mL GO + 0.1 mM $HAuCl_4$ in pH 9.0 PBS buffer solution at a scan rate of 50 mV/s. The black dash arrow and blue arrow indicate the scan direction and current changes direction, respectively.

3.2. Characteristics of the Modified Electrodes

As shown in Figure 2, SEM was used to characterize the morphology of the rGO-Au_{nano} sensing interface formed by electrochemical reduction. SEM imaging of the rGO-Au_{nano} deposited on a GCE showed a large amount of Au_{nano} evenly distributed on the substrate, which had a wrinkled texture associated with the presence of rGO sheets. The uniform distribution of Au_{nano} with an average diameter of ~30 nm indicated that rGO was formed with Au_{nano} by the electrochemical deposition, which effectively promoted the specific surface area of the sensing interface and allowed a large amount of Au_{nano} to be deposited on the electrode surface.

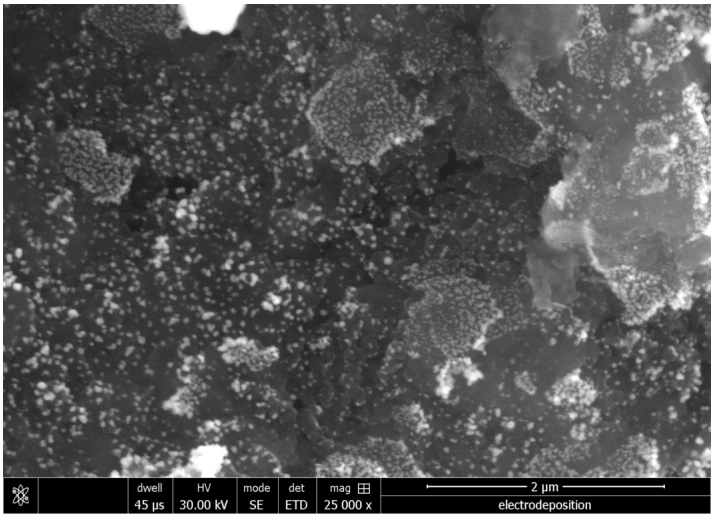

Figure 2. SEM image of rGO-Au_{nano}/GCE.

As shown in Figure 3, XRD analysis was carried out, and the XRD pattern was analyzed to investigate the monocrystalline nature of the nanoparticles formed by the electrochemical reduction of the gold salt. Four diffraction peaks appeared at 2θ = 38.2°, 44.5°, 65.6° and 78.6° in the XRD pattern, which were consistent with the (111), (200), (220) and (311) planes, respectively, of gold metal (International Center for Diffraction Data, ICDD No. 4-0783), suggesting that the product synthesized by electrodeposition contains pure crystalline gold. The Bragg reflection peaks of Au_{nano} clearly indicate a face-centered cubic monocrystalline structure, which is consistent with the crystalline structure of gold. The XRD pattern shows a very high Bragg reflection peak corresponding to the (111) lattice plane, indicating that Au_{nano} related to the (111) lattice plane was flat [29] on the planar surface.

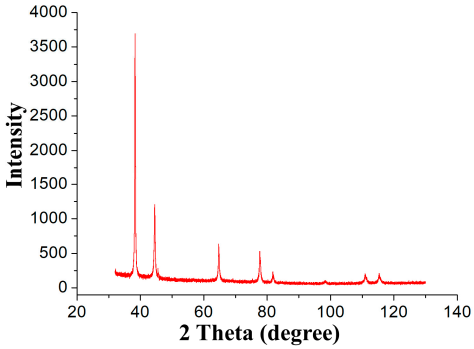

Figure 3. Representative XRD pattern of Au_{nano} synthesized by electrodeposition in a 0.1 mM $HAuCl_4$ solution.

The electron transfer characteristics of the surfaces of different electrodes were studied by CV using $[Fe(CN)_6]^{3-/4-}$ redox probes, as shown in Figure 4A. The $[Fe(CN)_6]^{3-/4-}$ redox currents on rGO/GCE were larger than those on the bare GCE. Additionally, the potential difference between the oxidation peak and reduction peak of the $[Fe(CN)_6]^{3-/4-}$ redox probe decreased because of the good electron transfer capability of rGO. The redox currents of the redox probes were further enhanced on rGO-Au_{nano}/GCE compared with those on bare GCE and rGO/GCE, which demonstrated that the presence of Au_{nano} in the rGO-Au_{nano} composite effectively improves the electron transfer capability.

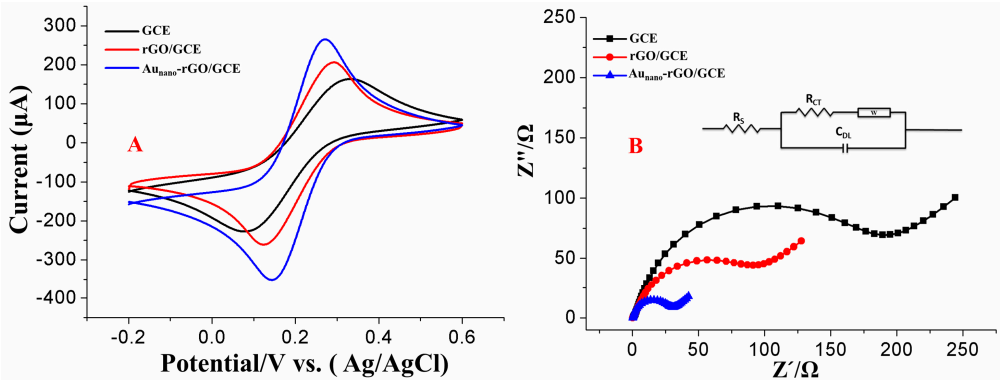

Figure 4. CV (**A**) and EIS (**B**) results for bare GCE, rGO/GCE and rGO-Au_{nano}/GCE in a solution of 5 mM $[Fe(CN)_6]^{3-/4-}$ containing 0.1 M KCl.

In this study, EIS, a common electrochemical characterization method that consists of low- and high-frequency regions corresponding to semicircular and linear portions, respectively, was also used to further investigate the electron transfer kinetics of the different electrodes, as shown in Figure 4B. Additionally, an equivalent circuit was used to fit the EIS data, as shown in Figure 4B, where Rct, Rs and C_{DL} represent the charge transfer resistance, resistance of solution and double layer capacitance, respectively. Among the three parameters, Rct is the most important key factor and is widely used for the characterization of electron transfer kinetics on the electrode surface. The semicircular and linear portions represent the Rct and the surface diffusion process, respectively, which reflects the electron transfer kinetics of $[Fe(CN)_6]^{3-/4-}$ at the electrode interface [30]. A smaller, well-defined semicircle was observed in the high-frequency region with rGO/GCE than in the region of bare GCE, which suggested that the presence of rGO reduced the impedance of the electrode interface [31]. The smallest R_{ct} value was observed with rGO-Au_{nano}/GCE because the corresponding diameter of the semicircle was the smallest, which suggested that the presence of Au_{nano} in the rGO layer can effectively improve the electron transfer kinetics of the electrode surface. The first EIS point of all the electrodes in the low-frequency region was almost the same, which indicated that Rs was the same for all the electrodes. These results were in good agreement with the CV results.

3.3. Optimization of the Experimental Conditions

In this study, the number of sweep segments, deposition time and deposition potential were investigated to determine the optimal experimental conditions for rGO-Au_{nano}/GCE that result in the highest detection sensitivity of As(III). The effect of deposition time on the stripping response was investigated in a nitric acid solution (0.1 M). The thickness of the rGO-Au_{nano} sensing composite, which could have a significant effect on the sensitivity, can be controlled by changing the number of electrodeposition cycles, i.e., the number of sweep segments. In this work, 4 to 18 sweep segments were tested to optimize the thickness of the sensing film, and the results can be seen in Figure 5A, which shows the As(III) stripping response with respect to the number of electrodeposition sweep segments. The stripping response of As(III) significantly increased with the number of sweep segments in the range from 4 to 10. This increase may be because the GCE surface was not saturated with rGO-Au_{nano} until the number of sweep segments reached 10. As the number of sweep segments was increased above 10, the stripping response of As(III) remained nearly constant. Thus, 10 sweep segments were used for further experiments.

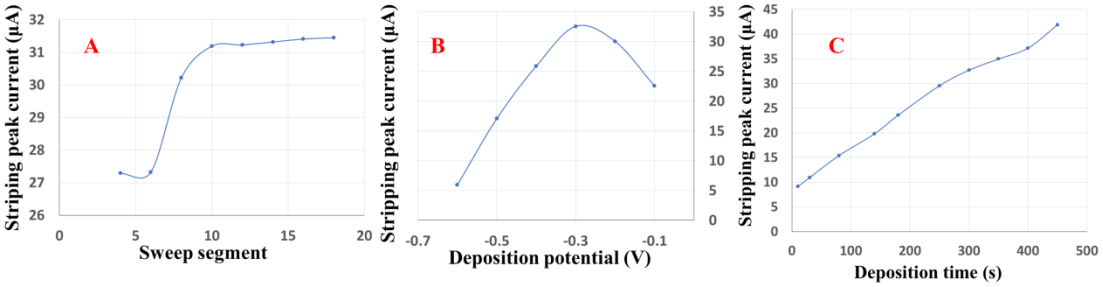

Figure 5. The effects of (**A**) the number of sweep segments, (**B**) the deposition potential and (**C**) the deposition time on the As(III) stripping peak currents on rGO-Au_{nano}/GCE in a 0.1 M HNO_3 solution containing 15 μg/L As(III).

As shown in Figure 5B, the deposition potential was optimized for the As(III) stripping response in the potential range from −0.1 to −0.6 V with a deposition time of 250 s. At a deposition potential of −0.3 V, the highest peak currents were obtained; thus, a deposition potential of −0.3 V was used for further analyses.

Additionally, the effect of the deposition time on the stripping response was investigated in the range from 10 to 450 s, as shown in Figure 5C. The stripping signals of As(III) sharply increased as the deposition time increased. Finally, a deposition time of 250 s was chosen for the following measurements as a compromise between sensitivity and analysis time.

3.4. Stripping Responses of Different Electrodes

The stripping responses of different electrodes, i.e., a bare GCE, rGO/GCE, Au_{nano}/GCE and rGO-Au_{nano}/GCE, were investigated under the optimum conditions. As shown in Figure 6, As(III) produced no obvious response on bare GCE and rGO/GCE. However, a significant As(III) response can be observed on Au_{nano}/GCE. A higher and sharper As(III) stripping response was obtained on rGO-Au_{nano}/GCE. The enhanced stripping response of rGO-Au_{nano}/GCE can be attributed to the following: (1) the electrodeposition of solution-state As(III) was enhanced due to the electrogeneration of H_2 near Au_{nano} by chemical reduction [11]; (2) rGO increased the specific surface area and conductivity of the sensing interface; and (3) the combined effect of Au_{nano} and rGO synthesized by electrochemical reduction imparted a very high sensitivity for As(III) detection [14]. The results show that the rGO-Au_{nano} sensing interface-modified GCE has outstanding sensitivity and is highly promising for application.

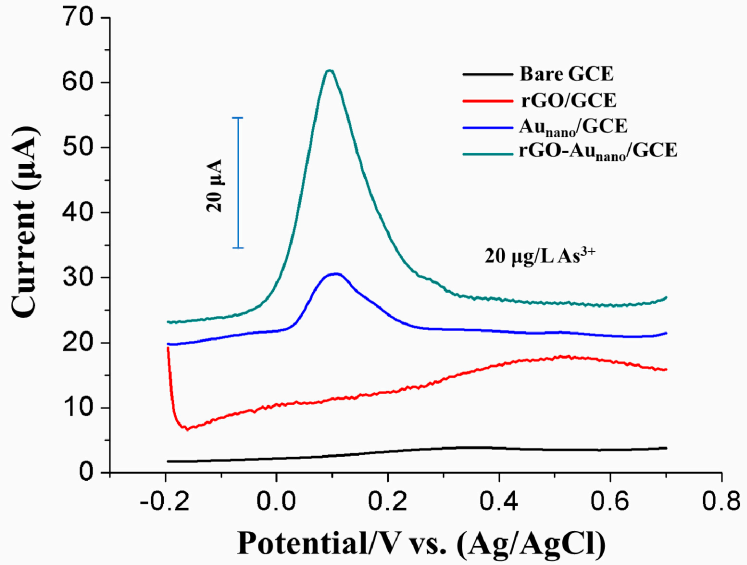

Figure 6. Comparison of SWASV curves for different modified electrodes used for the detection of 20 µg/L As(III) at a deposition potential of −0.3 V with a deposition time of 250 s in a 0.1 M nitric acid solution.

3.5. Analytical Performance of rGO-Au$_{nano}$/GCE

Under the optimal conditions, calibration curves for the stripping response of As(III) at both common and trace level concentrations were established. A series of SWASV As(III) responses and the corresponding calibration plots in the concentration range from 1 to 50 µg/L are shown in Figure 7A,B, respectively. The calibration curve and correlation coefficient were y = 1.521x + 7.89 (x: µg/L, y: µA) and 0.992, respectively. A significant and good linear relationship between the stripping peak current and the concentration of As(III) was obtained between 1.0 and 50.0 µg/L with a sensitivity of 1.521 µAµg/L. The SWASV As(III) responses in a lower concentration range, i.e., 0.1–1.2 µg/L, are shown in Figure 8A. The calibration curve and correlation coefficient were y = 10.597x − 0.401 (x: µg/L, y: µA) and 0.985, respectively. A detection limit of 0.08 µg/L was obtained according to the formula LOD = 3 σ/S, where σ is the standard deviation of a blank sample tested 10 times and S is the slope of the corresponding linear calibration equation of y = 1.521x + 7.89. The responses indicate that a higher sensitivity and lower LOD can be obtained by increasing the deposition time from 250 s to 800 s (Figure 8B). The specific stripping potential of As(III) changed as the As concentration changed from low to high. The peak shifting may be explained by the oxidation of additional As deposited on the electrode surface at a low positive potential with a high concentration of As(III). With a low concentration of As(III), only a trace amount of As was deposited on the electrode surface and was difficult to oxidize at a low positive potential; thus, the peak appeared at a more positive potential [32]. A comparison of the major analytical properties obtained in this work and those from previous work is shown in Table 1. Table 1 shows that the analytical performance of rGO-Au$_{nano}$/GCE is comparable and even better than that in previous reports, and this electrode is more controllable and easier to prepare and use and offers a lower limit of detection than other previously reported electrodes.

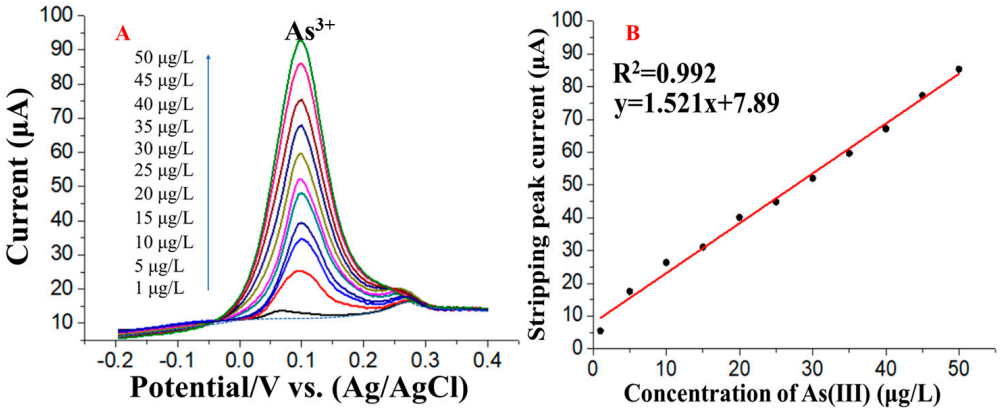

Figure 7. (**A**) SWASV response curves of rGO-Au_{nano}/GCE for the detection of different concentrations of As(III) and (**B**) the corresponding relationship between concentration and peak current in the concentration range from 1 μg/L to 50 μg/L (deposition time: 250 s).

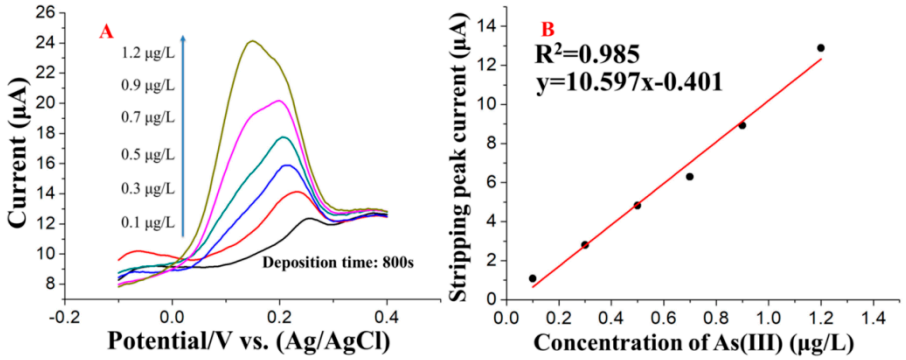

Figure 8. (**A**) SWASV response curves of rGO-Au_{nano}/GCE for the detection of different concentrations of As(III) and (**B**) the corresponding relationship between concentration and peak current in a concentration range from 0.1 μg/L to 1.2 μg/L (deposition time: 800 s).

Table 1. Comparison of different modified electrodes for the determination of As(III).

Electrodes	Technique	Linear Range (μg/L)	Detection Limit (μg/L)	Reference
Au-RGO/GCE	ASLSV	0.3–20	0.1	[14]
AuNP/BDD-modified electrode	SWASV	100–1500	20	[33]
nanoPt-Fe(III)/MWCNT/GCE	ASV	0–225	0.75	[34]
rGO-Fe_3O_4/SPCE	SWASV	2–20	0.3	[35]
Gold nanoparticle/GCE	ASV	0–15	0.25	[36]
AuNP-PCWEs	SWASV	2–50	2.2	[37]
rGO/Fe_3O_4/GCE	SWASV	0.1–20	0.12	[38]
Gold disk	SWASV	225–1800	3.7	[39]
Sub-BT/Au	DPASV	0–11.25	0.28	[40]
Nano-Au/GCE	LSV	3.675–87.075	1.8	[41]
I^--nano-Au/PANI/GCE	SWV	610–3050	0.4	[42]
rGO-Au_{nano}/GCE	SWASV	1–60	0.08	This work

ASLSV: anodic stripping linear sweep voltammetry, AuNP/BDD: gold nanoparticles on boron-doped diamond, MWCNT: multiwalled carbon nanotube, AuNP-PCWEs: gold nanoparticle-modified paper-based carbon working electrodes, rGO: reduced graphene oxide, BT: butanethiol, PANI: polyaniline.

3.6. Stability Measurements

As shown in Figure 9, to verify the suitability and reproducibility of rGO-Au_{nano}/GCE for As(III) determination, eight SWASV responses to 5 μg/L As(III) were obtained as continuous repetitive measurements. The times for each step were 250 s, 10 s, 4.8 s and 120 s for the deposition, standing,

stripping and cleaning steps, respectively. Thus, the total working time of the electrode in the solution for each measurement should be 384.8 s. The relative standard deviation of the eight repetitive measurements of As(III) was 1.178%, which is less than 20%, demonstrating the good reusability and stability of rGO-Au_{nano}/GCE for repeated SWASV measurements of As(III) under optimal conditions.

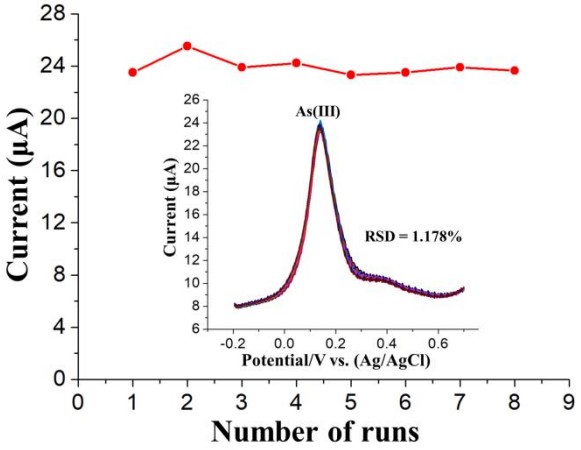

Figure 9. Eight repeated SWASV measurements of 5 μg/L As(III) with rGO-Au_{nano}/GCE. The insets correspond to the data collected from every SWASV curve for a total of eight measurements. RSD refers to the relative standard deviation.

3.7. Interference Studies

The influence of other ions, such as Na^+, K^+, Fe^{2+}, Mn^{2+}, Zn^{2+}, Mg^{2+}, Ca^{2+}, Pb^{2+} and Cd^{2+}, was also investigated in a synthetic solution containing 100-fold higher concentrations of the above nontarget ions than of As to estimate the possible influence of interference on the stripping response of trace As(III) under optimal conditions, as shown in Figure 10. The results demonstrated that the addition of nontarget ions had no significant effect on the As(III) stripping responses of the proposed electrode because the current mean values obtained in the presence of nontarget ions were within the $\pm 2 \times$ standard deviation range of the current measured in the absence of nontarget ions.

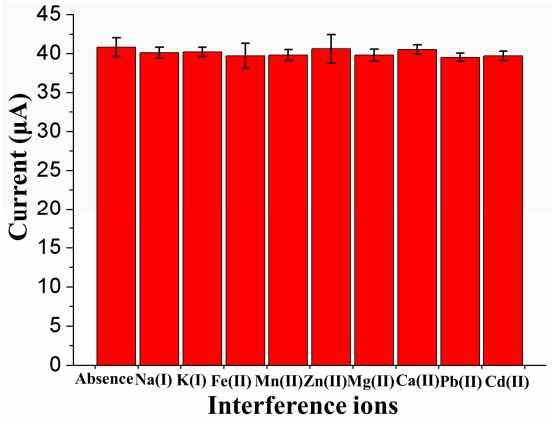

Figure 10. Interference study on the stripping peak currents of 15 μg/L As(III) in the presence of 10-fold higher concentrations of different ions.

3.8. Application to Real Sample Analysis

To investigate the practical application of the proposed sensor for the determination of As(III), several soil samples were analyzed under optimal conditions. Hydride generation atomic fluorescence spectrometry (HG-AFS) was used to verify the accuracy of the prepared electrochemical platform. The pretreatment process for the soil samples is described in Section 2.4, and the analysis was carried

out based on a standard addition method. The average recovery of As(III) was 98.97%, which demonstrated that the detection results obtained using the proposed platform were consistent with those obtained by HG-AFS (Table 2). To further verify the significant difference in accuracy between the proposed platform and HG-AFS, a paired t-test at the 95% confidence level was performed, and the results are presented in Table 2. Based on the statistical analysis results, we easily concluded that there was no significant difference between the two techniques because the $t_{calculated}$ of As(III) was below $t_{critical}$ (4.30 at 2 degrees of freedom). Therefore, the proposed modified electrode can be used for the analysis of As(III) at trace levels in real samples.

Table 2. Results of the detection of As(III) in soil sample extracts.

Sample No.	Added (μg/L)	Detected by SWASV [a] (μg/L)	Detected by HG-AFS [a] (μg/L)	$t_{calculated}$	Recovery (%)
1	-	13.57 ± 0.58 [b]	13.69 ± 0.22 [b]	1.95	-
	5.00	18.63 ± 0.74			101.20
	10.00	23.42 ± 0.60			98.50
2	-	18.62 ± 0.52	18.73 ± 0.23	1.73	-
	10.00	28.43 ± 0.49			98.10
	15.00	33.49 ± 0.62			99.13
3	-	15.38 ± 0.63	15.44 ± 0.41	1.62	-
	15.00	30.13 ± 0.41			98.33
	20.00	35.09 ± 0.73			98.55

[a] SWASV and HG-AFS measurements were repeated five times (n = 5). [b] Mean value ± standard deviation.

4. Conclusions

In this study, rGO-Au_{nano}/GCE was created by a one-step electrodeposition process with CV and used for the sensitive detection of As(III). The rGO-Au_{nano}/GCE sensor exhibits a better limit of detection than other Au_{nano}-based modified electrodes and is more controllable and stable. Additionally, the morphology, physical and chemical properties of the fabricated rGO-Au_{nano}/GCE were characterized by SEM, XRD, SWASV, EIS and CV. Parameters such as the deposition time, number of sweep cycles and deposition potential were optimized. The proposed rGO-Au_{nano}/GCE sensor shows very high sensitivity for the determination of As(III) based on the combined effects of rGO and $Au_{nano.}$ The rGO produced during electrodeposition effectively increases the specific surface area and electron transfer capability of the electrode. Additionally, rGO prevents the agglomeration of Au_{nano}, allowing good dispersal of Au_{nano} on the electrode surface and further improving the catalytic performance. A satisfactory recovery of As(III) in a soil sample analysis was obtained, which demonstrated that the rGO-Au_{nano}/GCE sensor may have potential promising applications for As(III) monitoring of environmental and food samples.

Author Contributions: G.Z. designed the experiments and wrote the paper. G.L. contributed reagents/materials/analysis tools.

Funding: This research was funded by the General Program of the National Natural Science Foundation of China (no. 31671578) and the National High Technology Research and Development Program of China (no. 2013AA102302).

Conflicts of Interest: The authors declare no conflict of interest.

References

1. Ning, Z.; Lobdell, D.T.; Kwok, R.K.; Liu, Z.; Zhang, S.; Ma, C.; Riediker, M.; Mumford, J.L. Residential exposure to drinking water arsenic in Inner Mongolia, China. *Toxicol. Appl. Pharmacol.* **2007**, *222*, 351–356. [CrossRef] [PubMed]
2. Smith, A.; Lopipero, P.; Chung, J.; Haque, R.; Hernandez, A.; Moore, L.; Steinmaus, C. Arsenic in drinking water and cancer risks estimated from epidemiological studies in Argentina, Chile, Taiwan and Japan. *Epidemiology* **2000**, *11*, 93.

3. Rodriguez-Lado, L.; Sun, G.; Berg, M.; Zhang, Q.; Xue, H.; Zheng, Q.; Johnson, C.A. Groundwater arsenic contamination throughout China. *Science* **2013**, *341*, 866–868. [CrossRef] [PubMed]
4. Smedley, P.L.; Kinniburgh, D.G. A review of the source, behaviour and distribution of arsenic in natural waters. *Appl. Geochem.* **2002**, *17*, 517–568. [CrossRef]
5. Yin, X.B.; Yan, X.P.; Jiang, Y.; He, X.W. On-line coupling of capillary electrophoresis to hydride generation atomic fluorescence spectrometry for arsenic speciation analysis. *Anal. Chem.* **2002**, *74*, 3720–3725. [CrossRef] [PubMed]
6. Aggett, J.; Aspell, A.C. The determination of arsenic(III) and total arsenic by atomic-absorption spectroscopy. *Analyst* **1976**, *101*, 341–347. [CrossRef] [PubMed]
7. Yan, X.P.; Kerrich, R.; Hendry, M.J. Determination of (ultra) trace amounts of arsenic(III) and arsenic(V) in water by inductively coupled plasma mass spectrometry coupled with flow injection on-line sorption preconcentration and separation in a knotted reactor. *Anal. Chem.* **1998**, *70*, 4736–4742. [CrossRef]
8. Zhao, G.; Wang, H.; Liu, G.; Wang, Z. Optimization of stripping voltammetric sensor by a back propagation artificial neural network for the accurate determination of Pb(II) in the presence of Cd(II). *Sensors* **2016**, *16*, 1540. [CrossRef]
9. Etesami, M.; Karoonian, F.S.; Mohamed, N. Electrochemical deposition of gold nanoparticles on pencil graphite by fast scan cyclic voltammetry. *J. Chin. Chem. Soc.* **2011**, *58*, 688–693. [CrossRef]
10. Xiao, L.; Wildgoose, G.G.; Compton, R.G. Sensitive electrochemical detection of arsenic(III) using gold nanoparticle modified carbon nanotubes via anodic stripping voltammetry. *Anal. Chim. Acta* **2008**, *620*, 44–49. [CrossRef]
11. Bu, L.; Gu, T.; Ma, Y.; Chen, C.; Tan, Y.; Xie, Q.; Yao, S. Enhanced cathodic preconcentration of As(0) at Au and Pt electrodes for anodic stripping voltammetry analysis of As(III) and As(V). *J. Phys. Chem. C* **2015**, *119*, 11400–11409. [CrossRef]
12. Tan, Y.; Li, Y.; Zhu, D. Fabrication of gold nanoparticles using a trithiol (thiocyanuric acid) as the capping agent. *Langmuir* **2002**, *18*, 3392–3395. [CrossRef]
13. Zhang, J.; Oyama, M. Gold nanoparticle arrays directly grown on nanostructured indium tin oxide electrodes: Characterization and electroanalytical application. *Anal. Chim. Acta* **2005**, *540*, 299–306. [CrossRef]
14. Li, W.W.; Kong, F.Y.; Wang, J.Y. Facile one-pot and rapid synthesis of surfactant-free Au-reduced graphene oxide nanocomposite for trace arsenic(III) detection. *Electrochim. Acta* **2015**, *157*, 183–190. [CrossRef]
15. Fukushima, M.; Yanagi, H.; Hayashi, S.; Suganuma, N. Fabrication of gold nanoparticles and their influence on optical properties of dye-doped sol-gel films. *Thin Solid Films* **2003**, *438*, 39–43. [CrossRef]
16. Dai, X.; Nekrassova, O.; Hyde, M.E.; Compton, R.G. Anodic stripping voltammetry of arsenic(III) using gold nanoparticle-modified electrodes. *Anal. Chem.* **2004**, *76*, 5924–5929. [CrossRef] [PubMed]
17. El-Deab, M.S.; Okajima, T.; Ohsaka, T. Electrochemical reduction of oxygen on gold nanoparticle-electrodeposited glassy carbon electrodes. *J. Electrochem. Soc.* **2003**, *150*, 851–857. [CrossRef]
18. Hau, N.Y.; Chang, Y.H.; Huang, Y.T.; Wei, T.C.; Feng, S.P. Direct electroplated metallization on indium tin oxide plastic substrate. *Langmuir* **2013**, *30*, 132–139. [CrossRef]
19. Hau, N.Y.; Chang, Y.H.; Feng, S.P. Kinetics study of silver electrocrystallization on (3-mercaptopropyl) trimethoxysilane-grafted indium tin oxide plastic substrate. *Electrochim. Acta* **2015**, *158*, 121–128. [CrossRef]
20. Feng, H.P.; Paudel, T.; Yu, B.; Chen, S.; Ren, Z.F.; Chen, G. Nanoparticle-Enabled Selective Electrodeposition. *Adv. Mater.* **2011**, *23*, 2454–2459. [CrossRef]
21. Zhao, G.; Wang, H.; Liu, G.; Wang, Z.; Cheng, J. Simultaneous determination of trace Cd(II) and Pb(II) based on Bi/Nafion/reduced graphene oxide-gold nanoparticle nanocomposite film-modified glassy carbon electrode by one-step electrodeposition. *Ionics* **2016**, *23*, 767–777. [CrossRef]
22. Liu, C.; Wang, K.; Luo, S. Direct Electrodeposition of Graphene Enabling the One-Step Synthesis of Graphene–Metal Nanocomposite Films. *Small* **2011**, *7*, 1203–1206. [CrossRef] [PubMed]
23. Dai, X.; Compton, R.G. Direct electrodeposition of gold nanoparticles onto indium tin oxide film coated glass: Application to the detection of arsenic(III). *Anal. Sci.* **2006**, *22*, 567–570. [CrossRef] [PubMed]
24. Krasnodêbska-Ostrêga, B.; Kowalska, J. Ultrasound-assisted acetic acid extraction of metals from soils. *J. Chem. Anal.* **2003**, *48*, 967–974.
25. Zhou, M.; Wang, Y.; Zhai, Y.; Zhai, J.; Ren, W.; Wang, F.; Dong, S. Controlled synthesis of large-area and patterned electrochemically reduced graphene oxide films. *Chem. Eur. J.* **2009**, *15*, 6116–6120. [CrossRef] [PubMed]

26. Shao, Y.; Wang, J.; Engelhard, M.; Wang, C.; Lin, Y. Facile and controllable electrochemical reduction of graphene oxide and its applications. *J. Mater. Chem. C* **2010**, *20*, 743–748. [CrossRef]
27. Guo, H.L.; Wang, X.F.; Qian, Q.Y.; Wang, F.B.; Xia, X.H. A green approach to the synthesis of graphene nanosheets. *ACS Nano* **2009**, *3*, 2653–2659. [CrossRef]
28. Chen, L.; Tang, Y.; Wang, K.; Liu, C.; Luo, S. Direct electrodeposition of reduced graphene oxide on glassy carbon electrode and its electrochemical application. *Electrochem. Commun.* **2011**, *13*, 133–137. [CrossRef]
29. Jin, R.; Cao, Y.C.; Hao, E.; Métraux, G.S.; Schatz, G.C.; Mirkin, C.A. Controlling anisotropic nanoparticle growth through plasmon excitation. *Nature* **2003**, *425*, 487–490. [CrossRef]
30. Wei, Y.; Kong, L.T.; Yang, R.; Wang, L.; Liu, J.H.; Huang, X.J. Electrochemical impedance determination of polychlorinated biphenyl using a pyrenecyclodextrin-decorated single-walled carbon nanotube hybrid. *Chem. Commun.* **2011**, *47*, 5340–5342. [CrossRef]
31. Chen, D.M.; Gao, Z.F.; Jia, J.; Li, N.B.; Luo, H.Q. A sensitive and selective electrochemical biosensor for detection of mercury(II) ions based on nicking endonuclease-assisted signal amplification. *Sens. Actuators B* **2015**, *210*, 290–296. [CrossRef]
32. Li, S.S.; Zhou, W.Y.; Jiang, M.; Guo, Z.; Liu, J.H.; Zhang, L.; Huang, X.J. Surface Fe(II)/Fe(III) Cycle Promoted Ultra-Highly Sensitive Electrochemical Sensing of Arsenic(III) with Dumbbell-Like Au/Fe_3O_4 Nanoparticles. *Anal. Chem.* **2018**, *90*, 4569–4577. [CrossRef] [PubMed]
33. Pungjunun, K.; Chaiyo, S.; Jantrahong, I.; Nantaphol, S.; Siangproh, W.; Chailapakul, O. Anodic stripping voltammetric determination of total arsenic using a gold nanoparticle-modified boron-doped diamond electrode on a paper-based device. *Microchim. Acta* **2018**, *185*, 324. [CrossRef] [PubMed]
34. Shin, S.H.; Hong, H.G. Anodic stripping voltammetric detection of arsenic(III) at platinum-iron(III) nanoparticle modified carbon nanotube on glassy carbon electrode. *Bull. Korean Chem. Soc.* **2010**, *31*, 3077–3083. [CrossRef]
35. Xie, Z.; Xu, J.; Xie, F.; Xiong, S. Electrochemical Detection of As(III) by a rGO/Fe_3O_4-modified Screen-Printed Carbon Electrode. *Anal. Sci.* **2016**, *32*, 1053–1058. [CrossRef] [PubMed]
36. Majid, E.; Hrapovic, S.; Liu, Y.; Male, K.B.; Luong, J.H.T. Electrochemical determination of arsenite using a gold nanoparticle modified glassy carbon electrode and flow analysis. *Anal. Chem.* **2006**, *78*, 762–769. [CrossRef] [PubMed]
37. Nunez-Bajo, E.; Blanco-López, M.C.; Costa-García, A.; Fernández-Abedul, M.T. Electrogeneration of Gold Nanoparticles on Porous-Carbon Paper-Based Electrodes and Application to Inorganic Arsenic Analysis in White Wines by Chronoamperometric Stripping. *Anal. Chem.* **2017**, *89*, 6415–6423. [CrossRef]
38. Devi, P.; Sharma, C.; Kumar, P.; Kumar, M.; Bansod, B.K.S.; Nayak, M.K.; Singla, M.L. Selective electrochemical sensing for arsenite using rGO/Fe_3O_4 nanocomposites. *J. Hazard. Mater.* **2017**, *322*, 85–94. [CrossRef]
39. Simm, A.O.; Banks, C.E.; Compton, R.G. Sonoelectroanalytical detection of ultra-trace arsenic. *Electroanalysis* **2005**, *17*, 335–342. [CrossRef]
40. Rahman, M.R.; Okajima, T.; Ohsaka, T. Selective detection of As(III) at the Au(111)-like polycrystalline gold electrode. *Anal. Chem.* **2010**, *82*, 9169–9176. [CrossRef]
41. Hossain, M.M.; Islam, M.M.; Ferdousi, S.; Okajima, T.; Ohsaka, T. Anodic Stripping Voltammetric detection of arsenic(III) at gold nanoparticle-modified glassy carbon electrodes prepared by electrodeposition in the presence of various additives. *Electroanalysis* **2008**, *20*, 2435–2441. [CrossRef]
42. Chowdhury, A.N.; Ferdousi, S.; Islam, M.M.; Okajima, T.; Ohsaka, T. Arsenic detection by nanogold/conducting-polymer-modified glassy carbon electrodes. *J. Appl. Polym. Sci.* **2007**, *104*, 1306–1311. [CrossRef]